THE JOURNAL OF PHYSICAL CHEMISTRY LETTERS
A JOURNAL OF THE AMERICAN CHEMICAL SOCIETY

pubs.acs.org/JPCL
Letter

Nuclear Quantum Effects on the Electronic Structure of Water and Ice

Margaret L. Berrens, Arpan Kundu, Marcos F. Calegari Andrade, Tuan Anh Pham, Giulia Galli, and Davide Donadio*

Cite This: J. Phys. Chem. Lett. 2024, 15, 6818−6825
Read Online

ACCESS | Metrics & More | Article Recommendations | Supporting Information

ABSTRACT: The electronic properties and optical response of ice and water are intricately shaped by their molecular structure, including the quantum mechanical nature of the hydrogen atoms. Despite numerous previous studies, a comprehensive understanding of the nuclear quantum effects (NQEs) on the electronic structure of water and ice at finite temperatures remains elusive. Here, we utilize molecular simulations that harness efficient machine-learning potentials and many-body perturbation theory to assess how NQEs impact the electronic bands of water and hexagonal ice. By comparing path-integral and classical simulations, we find that NQEs lead to a larger renormalization of the fundamental gap of ice, compared to that of water, ultimately yielding similar bandgaps in the two systems, consistent with experimental estimates. Our calculations suggest that the increased quantum mechanical delocalization of protons in ice, relative to water, is a key factor leading to the enhancement of NQEs on the electronic structure of ice.

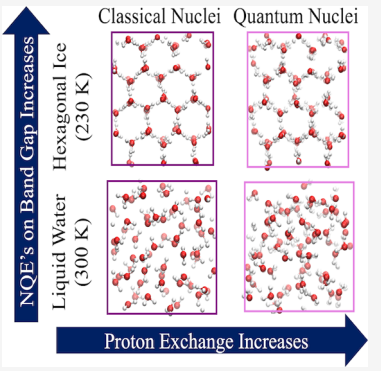

Water and ice provide a natural solvation environment for most chemical processes of atmospheric and biological importance. The electronic structure of water affects the chemistry of biological, geochemical, and environmental reactions, as well as the properties of energy conversion devices, such as photoelectrochemical cells.[1−4] Understanding the relation between the structural and electronic properties of water will help shed light on the chemistry of natural processes and aid the optimization of technological applications. There has been extensive research on the electronic properties of liquid water,[5−9] but significantly less attention has been directed toward the electronic structure of hexagonal ice (Ice I_h), water's most common solid form. A thorough understanding of its electronic structure is essential to elucidate the role of ice as a substrate or a catalyst in environmental chemistry[10−13] and astrochemistry.[14,15]

Data inferred from experiments and interpreted by Bischoff et al.[8] point at water and ice having similar fundamental gaps (E_g), despite considerable structural differences: 9.0 ± 0.2 for water[7,16−18] at room temperature and 9.4 ± 0.3 for ice[19−21] at 77 K. Interpreting experiments at the molecular level and connecting the structural and dynamical properties to the electronic structure of water and ice remain challenging tasks, especially due to the disordered and dynamic nature of these systems. Molecular dynamics (MD) simulations combined with electronic structure calculations offer a promising means to address this knowledge gap.[7] Whereas nuclei are treated as classical particles in first-principles MD (FPMD), the inclusion of nuclear quantum effects (NQEs) is necessary to describe the electron−phonon interactions affecting the properties of materials with light elements.[22−28] NQEs can be modeled using Feynman's path integrals (PIs) or related methods,[29−32] although at a substantially higher computational cost.

Using trajectories generated with the Vydrov and Van Voorhis (rVV10) van der Waals density functional,[33] path-integral MD (PIMD) simulations with 6 beads, and supercells with 32 water molecules, Chen et al. estimated the bandgap of water at 300 K using self-consistent GW calculations with a two-point exchange-correlation kernel.[6] They obtained aband gap of 9.8 and 8.9 eV without and with vertex corrections, respectively and in both cases a renormalization (ΔE_g^{NQE}) of −0.7 eV. A similar computational protocol was used by Tal et al.,[9] who, however, increased the number of frames over which they conducted MBPT calculations and slightly modified the treatment of the exchange-correlation Kernel, obtaining a band gap of 9.2 eV when using vertex corrections. Gaiduk et al. reported a bandgap of 10 eV with a ΔE_g^{NQE} of −0.5 eV, using G_0W_0 calculations starting from hybrid DFT (they used both range-separated (RSH) and self-consistent hybrids).[7] They conducted simulations with the MB-pol potential and PIMD with 32 beads and used 64 water molecule cells. The major difference between the results obtained by Tal et al.[9] and Gaiduk et al. originates from the different positions of the

Received: May 5, 2024
Revised: June 17, 2024
Accepted: June 21, 2024
Published: June 25, 2024

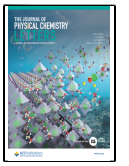

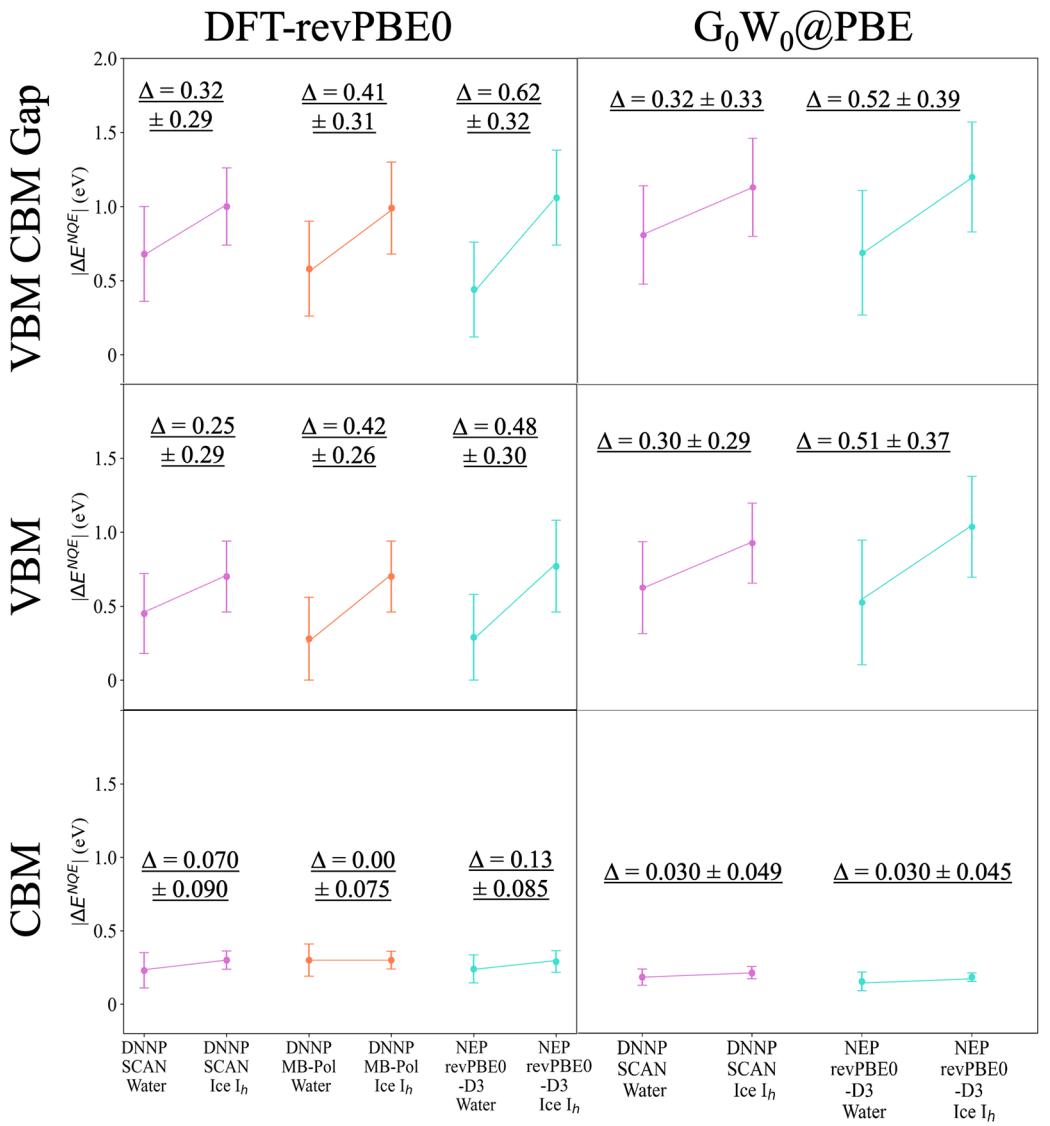

Figure 1. The difference between the fundamental gap obtained with classical and quantum trajectories (ΔE_g^{NQE}), upper panel, and the difference between the position of the VBM (middle panel) and CBM (lower panel) obtained with classical and quantum trajectories, for liquid water and ice I_h. The results in the left panels were obtained at the DFT level using the revPBE0 functional for 100 frames (left), and those in the right panels were obtained at the G_0W_0 level for 50 frames (right). The *x*-axis indicates the ML potentials used in the calculations. Δ represents the difference in ΔE_g^{NQE} between water and ice for each ML potential.

conduction band predicted in the two papers, while the positions of the valence bands are similar. For ice I_h, Engel et al. and Monserrat et al. estimated a large energy gap renormalization, −1.5 eV, using stochastic methods based on the quasi-harmonic approximation,[34,35] though the accuracy of these methods in a strong anharmonic regime is not guaranteed.[26,27,36] Bischoff et al. reported a band gap of ice of 9.8 and 9.3 eV (and that of water of 9.6 and 9.1 eV), depending on the type of self-consistent GW method used. In the case of ice, they applied just the zero-point renormalization (ZPR) obtained in refs 34 and 35 to electronic structure calculations at zero T, carried out for a Bernal−Fowler unit cell with 12 molecules.[8] The origin of the difference between the impact of the NQEs on the electronic properties of water and ice has not yet been clarified nor has ΔE_g^{NQE} been computed for ice by MD at finite temperatures. In addition, comparisons have been made for calculations carried out at different levels of electronic structure theory and with different structural models (different force fields and/or density functionals). Clearly, a fair and robust comparison calls for modeling the dynamical properties of water and ice at finite temperatures on an equal footing, using quantum simulations and computing the electronic structure of both systems within the same approximations. Such a comparison is still amiss.

In this Letter, we investigate the effect of NQEs on the electronic structure of water and ice I_h by carrying out MBPT calculations at the G_0W_0 level of theory for an ensemble of configurations obtained from classical and PIMD simulations, to provide a consistent estimate of the bandgap renormalization of both systems. Our calculations confirm that NQEs have a significantly larger effect on the electronic properties of ice I_h compared with those of liquid water. A comparative analysis of hydrogen-bonding configurations in water and ice suggests that the degree of transient proton transfer from hydrogen bond donors to acceptors is the key structural feature affecting the bandgap renormalization.

https://doi.org/10.1021/acs.jpclett.4c01315
J. Phys. Chem. Lett. 2024, 15, 6818−6825

We use machine learning potentials (MLPs) to accelerate both classical and PIMD simulations. We specifically employ two different MLPs derived from density functional theory (DFT) with two functionals: a van der Waals corrected hybrid functional (revPBE0-D3)[37−39] and the *strongly constrained and appropriately normed* (SCAN) exchange-correlation functional.[40] Using revPBE0-D3, we obtained a neural network potential fitted with an evolutionary algorithm ("neuro-evolution potential" - NEP).[41,42] This potential has been shown to reproduce accurately the thermodynamic properties of water and ice, including the density anomaly of water, and it is of similar quality as previously reported neural network models fitted on the same density functional. However, it is more computationally efficient.[43,44] In the case of the SCAN functional, we used a previously trained and validated deep neural network potential (DNNP) that accurately reproduces the structural[45] and vibrational[46] properties of water and ice. We compared the electronic structure results obtained for trajectories with two different MLPs to rule out systematic biases originating from a specific MLP scheme or the underlying density functional approach. The differences and similarities of the two underlying density functionals used in this work have been the focus of several *ab initio* MD studies and are briefly discussed in the Supporting Information.[47,48] Our results are further validated using trajectories generated with a DNNP fitted to the first-principles many-body force field MB-pol.[49]

We performed quantum simulations with a generalized Langevin equation thermostat (PIGLET),[50,51] which provides well-converged results, compared to PIMD, using a small number of beads (p = 8) in the ring-polymer.[52] MD simulations were carried out at 300 and 230 K for water and ice, respectively. A temperature of 230 K was chosen for ice to investigate the NQE on the electronic properties at environmentally relevant conditions. It is expected that as the temperature increases the gap will only slightly decrease for ice I_h.[53] For the PIGLET simulations, at 230 K, the average quantum kinetic and potential energies of ice are converged within 3 meV/atom with only 8 beads (Figure S2). Size effects on the calculated bandgap of liquid water were carried out by Gaiduk et al.[7] Here, we tested size effects on the bandgap of bulk ice using supercells with 96 and 192 molecules, which showed that a simulation cell of 96 water molecules is sufficient to obtain an estimate of the bandgap within the statistical uncertainty of our calculations (Table S2). The choice of system size in our MD simulations was mainly constrained by the cost of performing several tens of MBPT calculations over classical MD and PIMD trajectories.

Electronic structure calculations are performed using the G_0W_0 method on electronic structure calculations at the PBE[54] level of theory, for 50 equally spaced frames selected from MD and PIMD trajectories of 100 ps for water and ice, respectively (convergence as a function of the number of frames is shown in Figure S4). The electronic structure calculations from the PIMD runs were performed for a randomly chosen ring-polymer bead. All G_0W_0 calculations were carried out with the WEST code.[55] We note that G_0W_0@PBE underestimates the E_g of water, i.e. the energy difference between the conduction band minimum (CBM) and valence band maximum (VBM), of liquid water by approximately 1 eV lower, compared to higher level theories using hybrid functionals as starting points for MBPT and compared to experimental estimates.[5,7] The use of the quasiparticle self-consistent GW (QSGW) method that includes vertex corrections also yields larger gaps.[6,8] However, for liquid water, one-shot G_0W_0@PBE calculations yield an estimate of the effect of NQE on the electronic structure which is similar to that of the QSGW method.[6] Since the focus of this work is to estimate NQEs on the gap rather than the absolute values of the E_g, we utilized G_0W_0@PBE, which allowed us to sample a well-converged ensemble of configurations for relatively large systems.

The difference between the E_g of water and ice obtained with classical and quantum simulations, as well as the difference between the positions of the VBM and CBM, obtained from G_0W_0@PBE and hybrid calculations, are shown in Figure 1. Regardless of the underlying potential used for sampling and the electronic structure method, Figure 1 shows that NQEs considerably reduce the bandgap of both water and ice by raising the energy of the VBM and lowering, to a much smaller extent, the energy of the CBM. Consistent with previous findings, we find that NQEs have a much larger impact in ice, for which the ΔE_g^{NQE} amounts to 1.1 ± 0.32 to 1.2 ± 0.36 eV on the bandgap, which instead decreases by 0.70 ± 0.42 to 0.81 ± 0.33 eV in water. Hence, the larger NQEs in ice overall lead to a similar E_g for ice and liquid water, consistent with data inferred from experiments (9.0 ± 0.2 eV for water and 9.4 ± 0.3 eV for ice). Our results for ΔE_g^{NQE} are consistent with previous calculations for both water (−0.7 eV[6] and −0.5 eV[7]) and ice (−1.52 eV[34]). We note that the value for ice I_h in ref 34 was obtained for a configuration optimized at zero temperature. We find a similar bandgap renormalization with respect to a zero temperature optimized structure of 1.65 eV using the difference between a geometry-optimized structure and the band gap value obtained from the quantum DNNP@SCAN simulation at 230 K.

Overall, sampling with NEP enhances the difference in the NQEs-induced bandgap renormalization between ice and water, although it remains within the same uncertainty as the DNNP results. The error bars on the ΔE^{NQE} for the VBM are much larger than for the CBM. The main effect of quantum effects is not only to increase the energy of the VBM state, especially in ice, but also to broaden its energy distribution. In turn, the CBM is only slightly affected and does not undergo significant broadening.

Using the hybrid revPBE0 functional,[37−39] we verified that the trends reported above for ΔE^{NQE} for water and ice hold for trajectories generated with MB-pol data.[49,56−58] This model provides an accurate description of the structural, thermodynamic, dynamical, and spectroscopic properties of water.[49,59−61] Finally, the corresponding ΔE_g^{NQE}'s computed from the Kohn−Sham orbitals using the SCAN functional are reported in Figure S6. The values of the VBM and CBM energies from the MBPT and the Kohn−Sham DFT calculations are also reported in Tables S3, S4, and S5, respectively. We find that inexpensive DFT calculations (such as those using the SCAN functional) reproduce the trends for NQEs obtained from accurate MBPT, but unsurprisingly, MBPT is necessary to achieve bandgaps in reasonable agreement with experiments. As expected, the use of a hybrid exchange and correlation functional brings DFT calculations much closer to MBPT results, and the results for ΔE_g^{NQE} are within statistical uncertainty. The underestimation of the bandgap with revPBE0 can be in part attributed to the fact that the inverse of the appropriate fraction of exact exchange (α) in the hybrid functional is more than two times larger than that of the electronic dielectric constant (ε_∞) of water,[5] where it has

https://doi.org/10.1021/acs.jpclett.4c01315
J. Phys. Chem. Lett. 2024, 15, 6818−6825

been previously shown that the physical value of α can be related to $1/\varepsilon_\infty$ for a given material.[62]

To understand the effect of NQEs on the position of the VBM, we calculated the inverse participation ratio (IPR) for an ensemble of snapshots from either PIMD or classical MD simulations (Figure 2). The IPR of the ith Kohn–Sham orbital

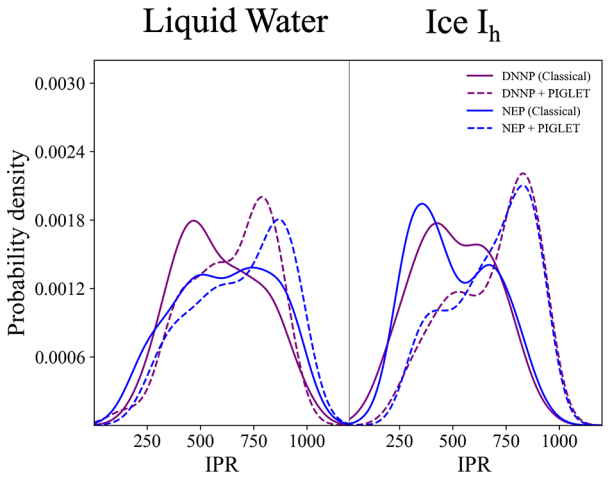

Figure 2. Probability density of the inverse participation ratio (IPR), fit with a Gaussian kernel density estimation, for the VB calculated with SCAN eigenstates and for liquid water (left) and ice (right). For each water system, we report the IPR for the DNNP with (dashed purple) and without (purple) NQEs and for the NEP with (dashded blued) and without (blue) NQEs. A higher IPR indicates stronger localization. The IPR values are scaled by 10000.

is calculated as $\int|\psi_i|^4 d^3r/(\int|\psi_i|^2 d^3r)^2$, where a higher IPR value corresponds to a more localized single-particle wave function. We calculated IPRs for the Kohn–Sham orbitals using the SCAN functional, including states within 50 meV of the VBM, which we refer to as the valence band (VB). For each water system and potential, we calculated the Gaussian kernel density estimation of the IPR for classical and quantum simulations. The histogram of IPR values for both the VB and the conduction band (CB) is reported in Figure S7. The IPR distribution for the VB spans values over 2 orders of magnitude larger than those for the CB, consistent with the known localized nature of occupied levels as opposed to delocalized empty levels. For both water and ice, the NQEs shift the VB distribution toward higher IPR values, indicating that quantum delocalization of the nuclei enhances the localization of the electronic levels. This phenomenon, previously observed in liquid water by Chen et al.,[6] was attributed to Anderson localization resulting from an increased disorder in the proton distributions, due to quantum fluctuations. The increased localization of electronic levels, akin to surface effects observed in water,[7] may also stem from the weakening of hydrogen bonds due to quantum delocalization. This is consistent with the known incorporation of NQEs, either strengthening or weakening of hydrogen bonds, depending on the local bonding environment.[63] Since water and ice have different cell sizes, we cannot compare the absolute shift of the IPR as the IPR depends on cell size. Therefore, we report a relative IPR shift with respect to the position of the peak of the IPR distribution in the classical simulation. For water and ice, there is an average shift in the relative peak position of the IPR distribution of the VB of 18% and 66%, respectively. The more pronounced shift for the VB of ice I$_h$ is responsible for the larger bandgap renormalization.

Previous studies investigating the NQEs on the structural properties of liquid water found that the inclusion of NQEs softens the local structure of water due to proton delocalization.[23] In particular, the oxygen–hydrogen and

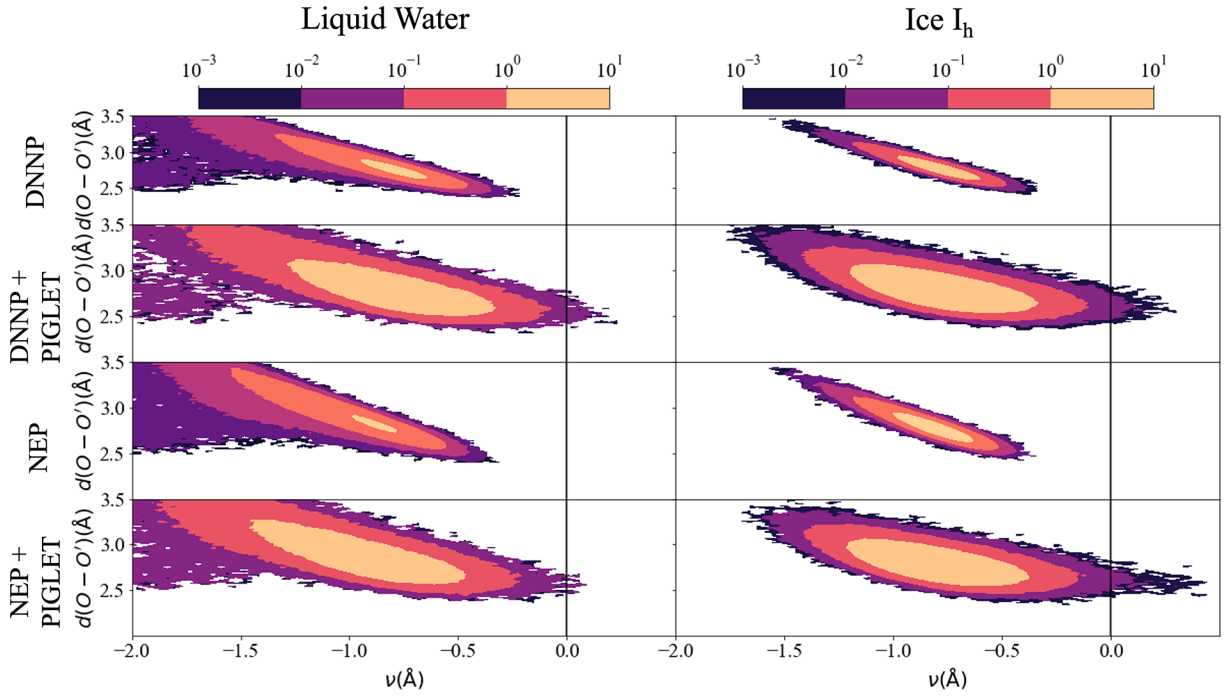

Figure 3. Joint probability distribution of the proton-transfer coordinate ν and the distance d(OO′) between the covalently bound and acceptor oxygen atoms for liquid water (left) and ice I_h (right). The top two rows are a comparison of the DNNP distributions with and without NQEs, and the bottom two rows are a comparison of the NEP distributions with and without NQEs.

https://doi.org/10.1021/acs.jpclett.4c01315
J. Phys. Chem. Lett. 2024, 15, 6818−6825

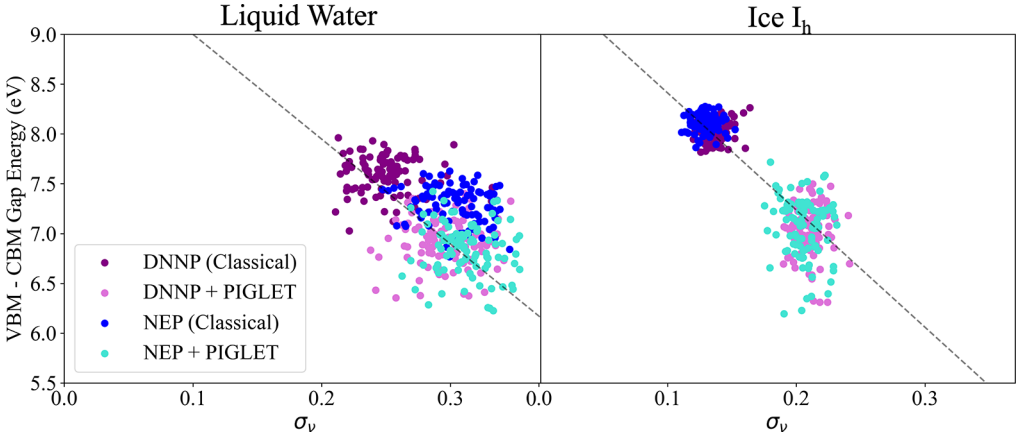

Figure 4. Scatter plot of the standard deviation in the proton transfer coordinate (σ_ν) for all hydrogen bonds in a given water system versus the corresponding VBM-CBM bandgap for a given frame calculated at the DFT level (revPBE0 functional) for liquid water (left) and ice I_h (right).

hydrogen−hydrogen radial distribution functions (g_{OH} and g_{HH}) exhibit the most apparent structural impact from NQEs. Specifically, the NQEs cause a broadening of the first two peaks of g_{OH}, which suggests a higher probability of proton transfer. The calculated radial and angular distribution functions in Figure S8 confirm that both MLPs reproduce these structural features for both water and ice. Similarly, NQEs cause a broadening of the distribution function of the H−O−H angle for water and ice. However, the causes of the difference in the NQE-induced bandgap renormalization between water and ice cannot be inferred from differences in radial distribution functions. To investigate why ΔE_g^{NQE} is much larger in ice I_h than in liquid water, we calculated the distributions of proton transfer coordinates and oxygen−oxygen distances for each hydrogen-bonded pair of water molecules (Figure 3) in our simulation cells. The proton transfer coordinate, defined as $\nu = d_{OH} - d_{O'H}$, represents the asymmetric stretch coordinate obtained from the difference between two oxygen-shared-hydrogen distances d_{OH} and $d_{O'H}$.[63−65] Incorporating NQEs in the simulations enhances hydrogen delocalization, yielding a small fraction of configurations with $\nu > 0$ that corresponds to short-lived autoprotolysis events. Here, for liquid water, we see that NQEs broaden the joint probability distribution $P(d_{OO'},\nu)$ with a tail extending into the $\nu > 0$ region. Comparing the distributions obtained with different MLPs and PIGLET, we observe a 2 times larger fraction of hydrogen bond configurations with $\nu > 0$ with the DNNP. In classical MD simulations, the probability distribution $P(d_{OO'},\nu)$ for ice I_h is much narrower than that of water. However, the inclusion of NQEs produces a broadening of the $P(dOO',\nu)$ distribution for ice, causing it to resemble that of water. Notably, this broadened distribution exhibits a higher likelihood of transient autoprotolysis in ice than in water after accounting for the NQEs.

To verify whether the observed change in the structure of the hydrogen bonds is responsible for the NQEs on E_g, we plot E_g (calculated at the DFT level with the revPBE0 functional) against the standard deviation of the proton transfer coordinate (σ_ν) for each snapshot; this coordinate is a measure of the spatial fluctuations in the proton transfer coordinates. Our results for classical and quantum simulations for both water and ice show that there is a correlation between the value of E_g and the proton fluctuations in the hydrogen bonds of the system, with a larger σ_ν associated with a lower bandgap.

When comparing water and ice, it is clear that for each system, a larger value of σ_ν correlates with lowered bandgaps. Significant distinctions in the distributions of σ_ν emerge between classical and quantum simulations for ice, with similar trends for both MLPs potential energy landscapes. In contrast, the distributions for liquid water exhibit not only considerably smaller disparities between classical and quantum simulations but also similar trends for both MLPs. These findings confirm that there exists a correlation between the fluctuations of protons in the hydrogen bond and the influence of NQEs on the bandgap. Previous investigations on liquid water[63] have also reported that NQEs induce substantial rearrangements in the positions of Wannier centers along a proton transfer coordinate, underscoring the pivotal role of proton delocalization in shaping the electronic structure of liquid water. Figure 4 highlights that NQEs exert an even more substantial impact on hydrogen bond fluctuations in ice I_h, consistent with their greater influence on the bandgap renormalization.

In summary, we have calculated the finite-temperature bandgap renormalization of water and ice I_h using many-body perturbation theory on ensembles of configurations generated using either classical MD or PIMD simulations and employing two different machine-learned potentials fitted to DFT forces obtained with meta-GGA or hybrid functionals. Consistent with earlier studies,[8] we find that nuclear quantum effects induce a significant decrease in the electronic bandgap of water and the in ice the reduction is even more pronounced, reaching twice the magnitude observed in water. As a consequence, water and ice I_h turn out to have similar fundamental gaps, consistent with data inferred from experiments. The two sets of simulations with different machine-learned potentials exhibit the same trends on nuclear quantum effects, albeit with a few quantitative differences, stemming from slight distinctions in the structural features of hydrogen bonds in classical simulations with the two potentials. A statistical analysis of the differences in the local structure of hydrogen bonds in quantum and classical simulations suggests that proton delocalization, and the resulting enhanced transient autoprotolysis, observed in PIMD simulations is sizably correlated with much larger NQEs on the bandgap renormalization of ice I_h, compared to water. These results highlight the critical importance of accounting for nuclear quantum effects when

https://doi.org/10.1021/acs.jpclett.4c01315
J. Phys. Chem. Lett. 2024, 15, 6818−6825

modeling the electronic properties of water and even more so of ice I_h. The observed influence of quantum proton delocalization and the ensuing bandgap renormalization are poised to have a considerable impact on molecular simulation studies examining ice as a solvation medium for environmental pollutants and as a catalyst for atmospheric chemistry reactions within snowpacks or clouds, a topic that has garnered increasing interest.[66−69]

■ ASSOCIATED CONTENT

Data Availability Statement

Data are available in the Materials Cloud Archive (www.materialscloud.org)[70] with ID materialscloud:2024.89, DOI:10.24435/materialscloud:pd-j6.

Supporting Information

The Supporting Information is available free of charge at https://pubs.acs.org/doi/10.1021/acs.jpclett.4c01315.

Computational methods, discussion of differences between MLPs, vibrational density of states, convergence of number of beads and number of frames used for electronic structure calculations, discussion of size effects on the proton transfer coordinate and bandgap values, a summary of calculated VBM CBM gap values, radial and angular distribution functions, histograms of IPR, and electronic density of states. (PDF)

Transparent Peer Review report available (PDF)

■ AUTHOR INFORMATION

Corresponding Author

Davide Donadio − *Department of Chemistry, University of California Davis, Davis, California 95616, United States;* orcid.org/0000-0002-2150-4182; Email: ddonadio@ucdavis.edu

Authors

Margaret L. Berrens − *Department of Chemistry, University of California Davis, Davis, California 95616, United States*

Arpan Kundu − *Pritzker School of Molecular Engineering, University of Chicago, Chicago, Illinois 60637, United States;* orcid.org/0000-0001-5351-3254

Marcos F. Calegari Andrade − *Quantum Simulations Group, Materials Science Division, Lawrence Livermore National Laboratory, Livermore, California 94550-5507, United States;* orcid.org/0000-0001-8630-7393

Tuan Anh Pham − *Quantum Simulations Group, Materials Science Division, Lawrence Livermore National Laboratory, Livermore, California 94550-5507, United States;* orcid.org/0000-0003-0025-7263

Giulia Galli − *Pritzker School of Molecular Engineering, University of Chicago, Chicago, Illinois 60637, United States; Department of Chemistry, University of Chicago, Chicago, Illinois 60637, United States; Materials Science Division and Center for Molecular Engineering, Argonne National Laboratory, Illinois 60439, United States;* orcid.org/0000-0002-8001-5290

Complete contact information is available at: https://pubs.acs.org/10.1021/acs.jpclett.4c01315

Notes

The authors declare no competing financial interest.

■ ACKNOWLEDGMENTS

We are grateful to Jiawei Zhan and Wenzhe Yu for their assistance with the G_0W_0 calculations and to Yifan Li for his assistance in the proton transfer coordinate calculations. We thank Francesco Paesani for useful suggestions about the choice of ML potentials. This work partly supported by the National Science Foundation under Grants No. 2305164 and No. 2053235 and by the Advanced Materials for Energy-Water Systems Center, an Energy Frontier Research Center funded by the U.S. Department of Energy, Office of Science, Basic Energy Sciences. Many body perturbation theory calculations were carried out with the WEST code, whose development is supported by MICCoM, as part of the Computational Materials Sciences Program funded by the U.S. Department of Energy, Office of Science, Basic Energy Sciences, Materials Sciences, and Engineering Division through Argonne National Laboratory, under Contract No. DE-AC02-06CH11357. G_0W_0 calculations have been performed using resources of the Argonne Leadership Computing Facility, which is a DOE Office of Science User Facility, supported by an ALCC grant. The work at the Lawrence Livermore National Laboratory was performed under the auspices of the U.S. Department of Energy under contract DE-AC52-07NA27344. M.F.C.A. and T.A.P. were supported as part of the Center for Enhanced Nanofluidic Transport, an Energy Frontier Research Center funded by the U.S. Department of Energy, Office of Science, Basic Energy Sciences, under award DE-SC0019112.

■ REFERENCES

(1) Zhong, J.; Kumar, M.; Anglada, J.; Martins-Costa, M.; Ruiz-Lopez, M.; Zeng, X.; Francisco, J. S. Atmospheric Spectroscopy and Photochemistry at Environmental Water Interfaces. *Annu. Rev. Phys. Chem.* **2019**, *70*, 45−69.

(2) Sverjensky, D. A.; Harrison, B.; Azzolini, D. Water in the deep Earth: The dielectric constant and the solubilities of quartz and corundum to 60kb and 1200°C. *Geochim. Cosmochim. Acta* **2014**, *129*, 125−145.

(3) Walter, M. G.; Warren, E. L.; McKone, J. R.; Boettcher, S. W.; Mi, Q.; Santori, E. A.; Lewis, N. S. Solar Water Splitting Cells. *Chem. Rev.* **2010**, *110*, 6446−6473.

(4) Grätzel, M. Photoelectrochemical cells. *Nature* **2001**, *414*, 338−344.

(5) Pham, T. A.; Zhang, C.; Schwegler, E.; Galli, G. Probing the electronic structure of liquid water with many-body perturbation theory. *Phys. Rev. B* **2014**, *89*, 060202.

(6) Chen, W.; Ambrosio, F.; Miceli, G.; Pasquarello, A. Ab initio Electronic Structure of Liquid Water. *Phys. Rev. Lett.* **2016**, *117*, 186401.

(7) Gaiduk, A. P.; Pham, T. A.; Govoni, M.; Paesani, F.; Galli, G. Electron affinity of liquid water. *Nat. Commun.* **2018**, *9*, 247.

(8) Bischoff, T.; Reshetnyak, I.; Pasquarello, A. Band gaps of liquid water and hexagonal ice through advanced electronic-structure calculations. *Phys. Rev. Res.* **2021**, *3*, 023182.

(9) Tal, A.; Bischoff, T.; Pasquarello, A. Absolute energy levels of liquid water from many-body perturbation theory with effective vertex corrections. *Proc. Nat. Acad. Sci.* **2024**, *121*, e2311472121.

(10) Grannas, A. M.; Pagano, L. P.; Pierce, B. C.; Bobby, R.; Fede, A. Role of Dissolved Organic Matter in Ice Photochemistry. *Environ. Sci. Technol.* **2014**, *48*, 10725−10733.

(11) Takenaka, N.; Bandow, H. Chemical Kinetics of Reactions in the Unfrozen Solution of Ice. *J. Phys. Chem. A* **2007**, *111*, 8780−8786.

(12) Grannas, A. M.; et al. An overview of snow photochemistry: evidence, mechanisms and impacts. *Atmos. Chem. Phys.* **2007**, *7*, 4329−4373.

(13) Klanova, J.; Klan, P.; Nosek, J.; Holoubek, I. Environmental Ice Photochemistry: Monochlorophenols. *Environ. Sci. Technol.* **2003**, *37*, 1568−1574.
(14) Mifsud, D. V.; Kaňuchová, Z.; Herczku, P.; Ioppolo, S.; Juhász, Z.; Kovács, S. T. S.; Mason, N. J.; McCullough, R. W.; Sulik, B. Sulfur Ice Astrochemistry: A Review of Laboratory Studies. *Space Sci. Rev.* **2021**, *217*, 14.
(15) Jenniskens, P.; Blake, D. F. Structural Transitions in Amorphous Water Ice and Astrophysical Implications. *Science* **1994**, *265*, 753−756.
(16) Bernas, A.; Ferradini, C.; Jay-Gerin, J.-P. On the electronic structure of liquid water: Facts and reflections. *Chem. Phys.* **1997**, *222*, 151−160.
(17) Winter, B.; Weber, R.; Widdra, W.; Dittmar, M.; Faubel, M.; Hertel, I. V. Full Valence Band Photoemission from Liquid Water Using EUV Synchrotron Radiation. *J. Phys. Chem. A* **2004**, *108*, 2625−2632.
(18) Ambrosio, F.; Miceli, G.; Pasquarello, A. Electronic Levels of Excess Electrons in Liquid Water. *J. Phys. Chem. Lett.* **2017**, *8*, 2055−2059.
(19) Campbell, M. J.; Liesegang, J.; Riley, J. D.; Leckey, R. C. G.; Jenkin, J. G.; Poole, R. T. The electronic structure of the valence bands of solid NH_3 and H_2O studied by ultraviolet photoelectron spectroscopy. *J. Phys. Chem. A* **1979**, *15*, 83−90.
(20) Shibaguchi, T.; Onuki, H.; Onaka, R. Electronic Structures of Water and Ice. *J. Phys. Soc. Jpn.* **1977**, *42*, 152−158.
(21) Baron, B.; Hoover, D.; Williams, F. Vacuum ultraviolet photoelectric emission from amorphous ice. *J. Chem. Phys.* **1978**, *68*, 1997−1999.
(22) Ceriotti, M.; Fang, W.; Kusalik, P. G.; McKenzie, R. H.; Michaelides, A.; Morales, M. A.; Markland, T. E. Nuclear Quantum Effects in Water and Aqueous Systems: Experiment, Theory, and Current Challenges. *Chem. Rev.* **2016**, *116*, 7529−7550.
(23) Markland, T.; Ceriotti, M. Nuclear Quantum Effects Enter the Mainstream. *Nat. Rev. Chem.* **2018**, *2*, 0109.
(24) Kundu, A.; Govoni, M.; Yang, H.; Ceriotti, M.; Gygi, F.; Galli, G. Quantum vibronic effects on the electronic properties of solid and molecular carbon. *Phys. Rev. Materials* **2021**, *5*, L070801.
(25) Kundu, A.; Song, Y.; Galli, G. Influence of nuclear quantum effects on the electronic properties of amorphous carbon. *Proc. Natl. Acad. Sci. U.S.A.* **2022**, *119*, e2203083119.
(26) Alvertis, A. M.; Engel, E. A. Importance of vibrational anharmonicity for electron-phonon coupling in molecular crystals. *Phys. Rev. B* **2022**, *105*, L180301.
(27) Kundu, A.; Galli, G. Quantum Vibronic Effects on the Electronic Properties of Molecular Crystals. *J. Chem. Theory Comput.* **2023**, *19*, 4011−4022.
(28) Kundu, A.; Galli, G. Quantum Vibronic Effects on the Excitation Energies of the Nitrogen-Vacancy Center in Diamond. *J. Phys. Chem. Lett.* **2024**, *15*, 802−810.
(29) Berne, B. J.; Thirumalai, D. On the Simulation of Quantum Systems: Path Integral Methods. *Annu. Rev. Phys. Chem.* **1986**, *37*, 401−424.
(30) Marx, D.; Parrinello, M. Ab initio path integral molecular dynamics: Basic ideas. *J. Chem. Phys.* **1996**, *104*, 4077−4082.
(31) Herrero, C. P.; Ramírez, R. Path-integral simulation of solids. *J. Phys.: Condens. Matter* **2014**, *26*, 233201.
(32) Huppert, S.; Plé, T.; Bonella, S.; Depondt, P.; Finocchi, F. Simulation of Nuclear Quantum Effects in Condensed Matter Systems via Quantum Baths. *Applied Sciences* **2022**, *12*, 4756.
(33) Sabatini, R.; Gorni, T.; de Gironcoli, S. Nonlocal van der Waals Density Functional Made Simple and Efficient. *Phys. Rev. B* **2013**, *87*, 041108.
(34) Engel, E. A.; Monserrat, B.; Needs, R. J. Vibrational renormalisation of the electronic band gap in hexagonal and cubic ice. *J. Chem. Phys.* **2015**, *143*, 244708.
(35) Monserrat, B.; Engel, E. A.; Needs, R. J. Giant electron-phonon interactions in molecular crystals and the importance of nonquadratic coupling. *Phys. Rev. B* **2015**, *92*, 140302.
(36) Kapil, V.; Engel, E.; Rossi, M.; Ceriotti, M. Assessment of Approximate Methods for Anharmonic Free Energies. *J. Chem. Theory Comput.* **2019**, *15*, 5845−5857.
(37) Perdew, J. P.; Ernzerhof, M.; Burke, K. Rationale for mixing exact exchange with density functional approximations. *J. Chem. Phys.* **1996**, *105*, 9982−9985.
(38) Adamo, C.; Barone, V. Toward reliable density functional methods without adjustable parameters: The PBE0 model. *J. Chem. Phys.* **1999**, *110*, 6158−6170.
(39) Grimme, S.; Antony, J.; Ehrlich, S.; Krieg, H. A consistent and accurate ab initio parametrization of density functional dispersion correction (DFT-D) for the 94 elements H-Pu. *J. Chem. Phys.* **2010**, *132*, 154104.
(40) Sun, J.; Ruzsinszky, A.; Perdew, J. Strongly Constrained and Appropriately Normed Semilocal Density Functional. *Phys. Rev. Lett.* **2015**, *115*, 036402.
(41) Fan, Z.; Zeng, Z.; Zhang, C.; Wang, Y.; Song, K.; Dong, H.; Chen, Y.; Ala-Nissila, T. Neuroevolution machine learning potentials: Combining high accuracy and low cost in atomistic simulations and application to heat transport. *Phys. Rev. B* **2021**, *104*, 104309.
(42) Chen, Z.; Berrens, M. L.; Chan, K.-T.; Fan, Z.; Donadio, D. Thermodynamics of Water and Ice from a Fast and Scalable First-Principles Neuroevolution Potential. *J. Chem. Eng. Data* **2024**, *69*, 128−140.
(43) Cheng, B.; Engel, A. E.; Behler, J.; Ceriotti, M. Ab initio thermodynamics of liquid and solid water. *Proc. Natl. Acad. Sci. U.S.A.* **2019**, *116*, 1110−1115.
(44) Schran, C.; Brezina, K.; Marsalek, O. Committee neural network potentials control generalization errors and enable active learning. *J. Chem. Phys.* **2020**, *153*, 104105.
(45) Zhang, L.; Wang, H.; Car, R.; E, W. Phase Diagram of a Deep Potential Water Model. *Phys. Rev. Lett.* **2021**, *126*, 236001.
(46) Sommers, G. M.; Calegari Andrade, M. F.; Zhang, L.; Wang, H.; Car, R. Raman spectrum and polarizability of liquid water from deep neural networks. *Phys. Chem. Chem. Phys.* **2020**, *22*, 10592−10602.
(47) Ohto, T.; Dodia, M.; Xu, J.; Imoto, S.; Tang, F.; Zysk, F.; Kühne, T. D.; Shigeta, Y.; Bonn, M.; Wu, X.; Nagata, Y. Accessing the Accuracy of Density Functional Theory through Structure and Dynamics of the Water-Air Interface. *J. Phys. Chem. Lett.* **2019**, *10*, 4914−4919.
(48) Palos, E.; Lambros, E.; Swee, S.; Hu, J.; Dasgupta, S.; Paesani, F. Assessing the Interplay between Functional-Driven and Density-Driven Errors in DFT Models of Water. *J. Chem. Theory Comput.* **2022**, *18*, 3410−3426.
(49) Bore, S.; Paesani, F. Realistic phase diagram of water from "first principles" data-driven quantum simulations. *Nat. Commun.* **2023**, *14*, 3349.
(50) Ceriotti, M.; Manolopoulos, D. E. Efficient First-Principles Calculation of the Quantum Kinetic Energy and Momentum Distribution of Nuclei. *Phys. Rev. Lett.* **2012**, *109*, 100604.
(51) Kapil, V.; et al. i-PI 2.0: A universal force engine for advanced molecular simulations. *Comput. Phys. Commun.* **2019**, *236*, 214−223.
(52) Kapil, V.; Behler, J.; Ceriotti, M. High order path integrals made easy. *J. Chem. Phys.* **2016**, *145*, 234103.
(53) Engel, E. A.; Monserrat, B.; Needs, R. J. Vibrational effects on surface energies and band gaps in hexagonal and cubic ice. *J. Chem. Phys.* **2016**, *145*, 044703.
(54) Perdew, J. P.; Burke, K.; Ernzerhof, M. Generalized Gradient Approximation Made Simple. *Phys. Rev. Lett.* **1996**, *77*, 3865−3868.
(55) Govoni, M.; Galli, G. Large Scale GW Calculations. *J. Chem. Theory Comput.* **2015**, *11*, 2680−2696.
(56) Medders, V.; Babin, G. R.; Paesani, F. Development of a "First-Principles" Water Potential with Flexible Monomers. III. Liquid Phase Properties. *J. Chem. Theory Comput.* **2014**, *10*, 2906−2910.
(57) Babin, V.; Medders, G. R.; Paesani, F. Development of a "First Principles" Water Potential with Flexible Monomers. II: Trimer Potential Energy Surface, Third Virial Coefficient, and Small Clusters. *J. Chem. Theory Comput.* **2014**, *10*, 1599−1607.

https://doi.org/10.1021/acs.jpclett.4c01315
J. Phys. Chem. Lett. 2024, 15, 6818−6825

(58) Babin, V.; Leforestier, C.; Paesani, F. Development of a "First Principles" Water Potential with Flexible Monomers: Dimer Potential Energy Surface, VRT Spectrum, and Second Virial Coefficient. *J. Chem. Theory Comput.* **2013**, *9*, 5395−5403.
(59) Cole, W. T. S.; Farrell, J. D.; Wales, D. J.; Saykally, R. J. Structure and torsional dynamics of the water octamer from THz laser spectroscopy near 215μm. *Science* **2016**, *352*, 1194−1197.
(60) Moberg, D. R.; Straight, S. C.; Knight, C.; Paesani, F. Molecular Origin of the Vibrational Structure of Ice I_h. *Chem. Lett.* **2017**, *8*, 2579−2583.
(61) Medders, G. R.; Paesani, F. Dissecting the Molecular Structure of the Air/Water Interface from Quantum Simulations of the Sum-Frequency Generation Spectrum. *J. Am. Chem. Soc.* **2016**, *138*, 3912−3919.
(62) Marques, M. A. L.; Vidal, J.; Oliveira, M. J. T.; Reining, L.; Botti, S. Density-based mixing parameter for hybrid functionals. *Phys. Rev. B* **2011**, *83*, 035119.
(63) Ceriotti, M.; Cuny, J.; Parrinello, M.; Manolopoulos, D. E. Nuclear quantum effects and hydrogen bond fluctuations in water. *Proc. Natl. Acad. Sci. U.S.A.* **2013**, *110*, 15591−15596.
(64) Tuckerman, M. E.; Marx, D.; Klein, M. L.; Parrinello, M. On the Quantum Nature of the Shared Proton in Hydrogen Bonds. *Science* **1997**, *275*, 817−820.
(65) Fritsch, S.; Potestio, R.; Donadio, D.; Kremer, K. Nuclear Quantum Effects in Water: A Multiscale Study. *J. Chem. Theory Comput.* **2014**, *10*, 816−824.
(66) Bartels-Rausch, T.; et al. A review of air−ice chemical and physical interactions (AICI): liquids, quasi-liquids, and solids in snow. *Atmos. Chem. Phys.* **2014**, *14*, 1587−1633.
(67) Bononi, F. C.; Chen, Z.; Rocca, D.; Andreussi, O.; Hullar, T.; Anastasio, C.; Donadio, D. Bathochromic Shift in the UV−Visible Absorption Spectra of Phenols at Ice Surfaces: Insights from First−Principles Calculations. *J. Phys. Chem. A* **2020**, *124*, 9288−9298.
(68) Berrens, M. L.; Chen, Z.; Chan, K.-T.; Anastasio, C.; Donadio, D. Solvation Structure and UV-Visible Absorption Spectra of the Nitrate Anion at the Air−Ice Interface by First-Principles Molecular Simulations. *ACS Earth Space Chem.* **2023**, *7*, 1761−1769.
(69) Loerting, T.; Voegele, A. F.; Tautermann, C. S.; Liedl, K. R.; Molina, L. T.; Molina, M. J. Modeling the heterogeneous reaction probability for chlorine nitrate hydrolysis on ice. *J. Geophys. Res.* **2006**, *111*, D14307.
(70) Talirz, L.; et al. Materials Cloud, a platform for open computational science. *Sci. Data* **2020**, *7*, 299.

https://doi.org/10.1021/acs.jpclett.4c01315
J. Phys. Chem. Lett. 2024, 15, 6818−6825